Atmósfera (1998) 11, pp. 43-73

A numerical investigation of a simple spectral atmospheric model

P. MARCUSSEN and A. WIIN-NIELSEN

Geophysical Department, University of Copenhagen, Juliane Maries Vej 30, 2100 Copenhagen, Denmark

(Manuscript received May 21, 1998; accepted in final form August 17, 1998)

RESUMEN

Para simular un número de fenómenos atmosféricos, se usa un modelo cuasinodivergente de dos niveles, que consta de 12 componentes espectrales en un plano-beta rectangular. El modelo no-lineal contiene dos componentes que describen el flujo zonal a cada nivel permitiendo vientos zonales con dos máximos y dos mínimos. Los campos torbellinarios a los dos niveles contienen cuatro componentes elegidas de tal manera que los campos torbellinarios tienen transportes de calor sensible y momento. El modelo permite una descripción completa de generaciones de energía, conversiones y disipaciones, porque las componentes torbellinarias son elegidas con tales números de onda que tienen lugar interacciones entre los torbellinos y los campos zonales. Calentamiento diabático, efectos topográficos y disipación de energía cinética son tomados en cuenta por el modelo. Una limitante del mismo es que consta de solamente un número de onda en la dirección zonal.

El modelo se usa para ilustrar desarrollos no-lineales de ondas baroclínicas, en varias escalas horizontales, en un caso de forzamiento sobre sólo las componentes zonales. Con un canal largo es posible simular el desarrollo de ondas largas, estacionarias, forzadas por la topografía y/o el calentamiento. Para definiciones especiales del calentamiento en ambos modos zonal y torbellinario, uno puede simular la formación y conservación de las situaciones de bloqueo, como resultado de las interacciones entre las componentes zonales y los torbellinos.

Las componentes torbellinarias normalmente entrarán en movimiento periódico o cuasiperiódico en el dominio de fases, a menos que el modelo esté forzado por el calentamiento, la topografía y la fricción. Dichos movimientos no forzados y sus periodos son investigados. Demostramos, asimismo, que el tipo de circulación atmosférica puede cambiar significativamente, en función de la posición del calentamiento máximo en la dirección sur-norte, ilutrando un cambio de sencillo a doble chorro y la alteración resultante en la intensidad y posición de las ondas.

ABSTRACT

A two-level quasi-nondivergent model containing 12 spectral components on a rectangular beta-plane is used to simulate a number of atmospheric phenomena. The nonlinear model contains two components that describe the zonal flow at each level permitting zonal winds with two maxima and two minima. The eddy fields at the two levels contain four components selected in such a way that the resulting eddy fields have transports of both sensible heat and momentum. The model permits a full description of energy generations, conversions and dissipations, because the eddy components are selected with such wave numbers that interactions take place between the eddies and the zonal fields. Diabatic heating, topographical effects and dissipation of kinetic energy are included in the model. A limitation of the model is that it contains only one wave number in the zonal direction.

The model is used to illustrate nonlinear developments of baroclinic waves on various horizontal scales in a case of forcing on the zonal components alone. With a long channel it is possible to simulate the development of long stationary waves forced by topography and/or heating. For special definitions of the heating on both the zonal and the eddy modes one may simulate the formation and maintenance of blocking situations as a result of interactions between the zonal components and the eddies. The eddy components will normally go into periodic or almost periodic motion in the phase domain unless the model is forced by heating, topography and friction. These unforced motions and their periods are investigated. We also show that the type of atmospheric circulation may change significantly as a function of the position of the maximum heating in the south-north direction, illustrating a change from single to double jets and the resulting change in the intensity and position of the waves.

1. Introduction

The atmosphere is a nonlinear system. Nevertheless, most of the theories represented in the standard textbooks are linear and based on perturbation theory. While the linear theory has given much insight in the creation of a number of atmospheric structures, it is based on the theory of small perturbations. As long as this theory is applied to stability investigations we face the problem that unstable perturbations grow exponentially. Therefore, after a certain time they will violate the basic assumptions of the theory, i.e the neglect of second order terms. Various attempts exemplified by the investigations of Charney (1959), Stuart (1960), Watson (1960) and Yang (1967) have been made to expand the investigations to include at least some aspects of nonlinearity.

The full nonlinear properties of the atmosphere are incorporated in prediction models and the models of the general circulations, also called climate models. Global, multilevel models, containing all aspects of external forcing and dissipation through parameterized processes, are used for short- and medium-range forecasting, for simulating the present climate and for investigations of certain limited aspects of climate change. The design of such models requires a specification of topographical effects and a number of other physical processes that contribute to the forcing of the atmosphere. The aim of these models is therefore to be as realistic as possible.

When it comes to the understanding of the essential physical processes driving the atmosphere, we should recall that the advanced general circulation models are almost as complicated as the atmosphere itself. A detailed analysis of the model output is necessary in order to compare the model behavior with the atmosphere. It may thus be very difficult to isolate the essential mechanisms for the creation of specific atmospheric structures and their change in time. For this reason one may be motivated to develop simplified models with only a few degrees of freedom as compared to the very large number of degrees of freedom of the global comprehensive models. With the help of such low-order models it is possible to achieve an increased understanding of various elements of the atmospheric system.

Quite a number of low-order models have been created over the last 3 to 4 decades starting with an extremely simple model by Lorenz (1960), who arrived at a maximum simplification of the dynamic equations for convection between two horizontal plates. A barotropic six component model used both for a stability analysis and for numerical integrations was designed by Wiin-Nielsen (1961). The famous three component model (Lorenz, 1963) leading to the strange attractor and to the concept of limited predictability of nonlinear systems, identical to chaos, created a general interest in nonlinear systems and their behavior in several branches of physics. Other simple models with forcing and dissipation were formulated and analysed for multiple steady states and their stability (Wiin-Nielsen, 1975, Charney and DeVore, 1979 and Wiin-Nielsen, 1979). The last two papers also attempted to create an understanding of the blocking phenomenon as a result of forcing by topography or heating. The block appeared as a high amplitude, stable steady state created by a nonlinear interaction between the zonal current and the waves. At a later time (Christensen, 1984 and Christensen and Wiin-Nielsen, 1996) it was shown that blocking could also be created as a nonlinear phenomenon through the interaction among the planetary waves with wave numbers 1, 2 and 3.

Low-order models may be designed for various kinds of geometry. The rectangular beta-plane has been used many times. Platzman (1960) formulated the barotropic vorticity equation on the sphere by using spherical harmonics as a set of orthogonal functions for this domain. Lorenz (1962) used low-order models to explain the essential aspects of rotating basin experiments and gave an explanation of vacillations. Wiin-Nielsen (1990, 1991a, 1991b, 1994a, 1994b) used a number of these models to discuss the atmospheric flow and its response to heating and topography on the Earth and on Mars. All these models were, however, simplified in such a way

that they contain either the transport of sensible heat or the transport of momentum by the atmospheric waves, but not both of them in the same model. A main purpose of the present paper is to present a low-order, nonlinear, baroclinic two-level model containing both of these important transport processes.

The model will be able to include the effects of topography, heating and dissipation in simple formulations. The inclusion of eddy momentum transports requires at least two meridional wave numbers at each level in a spectral formulation. The wave numbers describing the zonal part of the flow should be selected in such a way that they will interact with the eddy components. To achieve this will require the inclusion of 8 components (4 at each level) in the real domain of both trigonometric functions. At each level we shall need two components to describe the zonal flow. Consequently, we require 12 components for the minimal model. Since the model includes heating, topography and dissipation it is also a minimal model for the description of all the processes in the energy diagram formulated by Lorenz (1955). The spectral components are selected in such a way that the boundary conditions at the northern and southern walls are satisfied, while the flow is periodic in the west-east direction.

A model of the above kind will be able to give a schematic flow pattern only. A limitation of the model is that it permits only wind profiles that are symmetric around the middle of the channel. Having only one wave number in the west-east direction the maps of the streamfunction will at most have a single low and a single high for a given value of the south-north coordinate. No attempt has been made in the present paper to analyse the model for barotropic/baroclinic stability using analytical methods. Some aspects of instability for a low-order, barotropic model may be found in a paper by Marsh *et al.* (1995). With respect to the periodic behavior of large-scale waves we refer to the paper by Christensen and Wiin-Nielsen (1996) and by Wiin-Nielsen (1997).

2. Brief description of the model

No detailed description of the derivation of the model equations will be given in the paper because it follows standard procedures using orthogonal sets of functions. All model equations are, however, given in detail in the appendix, including all the quantities that are constants in a specific integration. The length of the beta-plane is L and the width is D. The basic wave numbers are $k = 2\pi/L$ and $\lambda = \pi/D$. The meridional wave numbers included in the eddies are wave numbers 1 and 3, while the wave numbers in the zonal flow are 2 and 4 as specified in eq. (3) to (6) in the appendix. The specific form in which we have written the streamfunctions for both the zonal flow and the eddies is such that the dependent variables in the model have the dimension of velocities measured in m per s. The equations in the appendix are written without the terms related to heating, topography and dissipation, but the terms necessary to be added to the right hand sides of the basic equations are given separately.

Subscripts 1 and 3 refer to the two levels which are located at 250 and 750 hPa, respectively. As is custommary we have added and subtracted the two basic equations. The subscripts * and T refer to half the sum and half the difference between the same quantities at levels 1 and 3.

Using the model for a specific purpose it is necessary to specify the length and the width of the channel and the six components of the heating and the mountain heigth to be used in the integration. The values of the coefficients specifying the dissipation have been the same in the examples given in the paper. All integrations have been carried out using Heun's scheme for the time integration. Normally, we have used a timestep of one hour, but in extreme cases it has occasionally been necessary to decrease the size of the timestep to secure numerical stability. The total length of the integration varies from case to case. Normally we have started all integrations

from a state of rest. This procedure requires a spin-up time, and since we are interested in reaching a possible steady state integrations can be quite long. Frequently it required a total integration time corresponding to 2 years.

For each integration graphs have been prepared showing the development of the wind components, the zonal and eddy forms of the available potential and the kinetic energy, and the generations, conversions and dissipations of these energies. Energy diagrams are given for specific times or for the average over a period. While examples of these figures are given later in the paper we have abstained from producing a very large number of figures to illustrate the examples. The model may be used in two slightly different forms. One of these contain the heating itself, while the other has been formulated using a Newtonian form of heating as given at the end of the appendix. The use of the two forms is determined by the problem under consideration.

3. The creation of waves

From the classical linear theory we know that baroclinic waves will be generated for certain wavelengths if the vertical wind shear is sufficiently large. Using a two-level, quasi-nondivergent model it is found that very short waves are stable due to the effects of the static stability, and that very long waves are stable due to the beta-effect. We know also from linear theory that barotropic flow is unstable for sufficiently large horizontal wind shears. It is therefore natural to let the first numerical experiment with the present low-order model deal with the extention of these linear theories into the nonlinear domain.

In the first example we shall look at the creation of waves using a forcing that appear on the first component z_{Tf} only (see the section on heating terms in the appendix). Such an experiment is similar to the famous experiment carried out by Phillips (1956). He used a simple linear heating function with heating in the southern and cooling in the northern half of the region. In our case the heating is on a single trigonometric component. We expect then that the heating will gradually create a growing temperature gradient which eventually will be so large that barotropic/baroclinic waves are created. In the first experiment we use $z_{Tf} = 20$ m per s, and we set the wavelength equal to 6000 km.

Figure 3.1 shows the streamfunction after 2900 time steps. It is seen that a well developed wave pattern has been created. An investigation of the development in time indicates that the waves are transient. However, Figure 3.2 containing the zonal available potential and the zonal kinetic energies, indicate that these two forms of energy become almost constant after about 4000 time steps. As shown in Figure 3.3 the same statement can be made for the eddy available potential and the eddy kinetic energies. This means that the transient waves should be almost periodic. Figure 3.4 shows that this is indeed the case since the component E_{*1} plotted against F_{*3} results in a closed curve.

We reproduce in Figure 3.5 the energy diagram for the experiment where it should be noted that a negative number means that the energy flow is in the opposite direction of the arrow in the figure. We notice that the energy diagram with respect to the directions is in agreement with those obtained from observational studies and especially that the energy conversion C (K_e, K_z) is positive and, thus, gives a contribution to the maintenance of the zonal flow. On the other hand, the amounts given in the diagram are typically smaller than those based on observations. One obvious reason is, of course that only one west-east component is contained in the model, but the results depends also on the choice of the west-east wavelength.

For this reason the experiment was repeated with a wavelength of 4000 km. Figure 3.6 shows the diagram, and in this case we note that the generations, conversions and dissipations

are generally larger than in the previous case although the directions are the same in the two figures.

It may also be of interest to test whether or not very long waves are stable in this example. An integration with $z_{Tf} = 20$ m per s and $L = 14000$ km was integrated with the result that no waves were generated during an integration of 180 days. Similar integrations with the same forcing, but for wavelengths of 1000 km and 2000 km showed that no waves were generated in these cases.

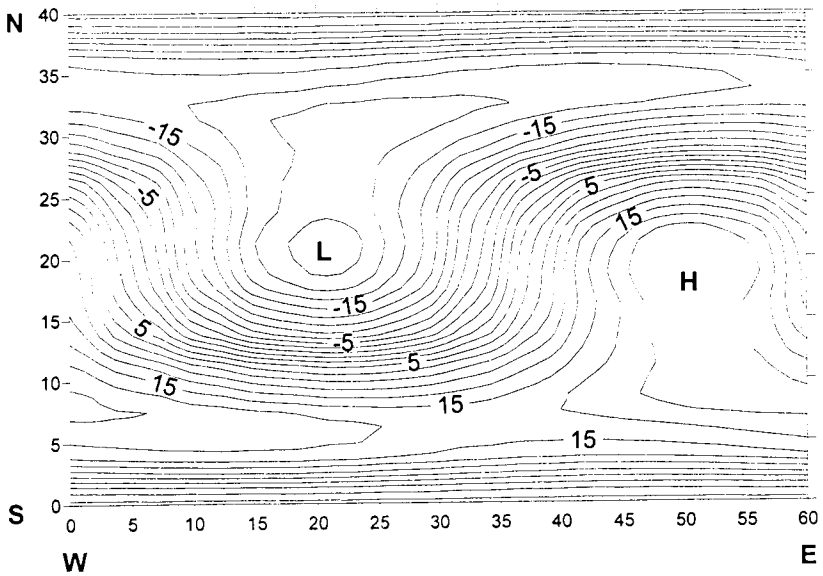

Fig. 3.1. Streamfunction after 2900 time steps with $z_{Tf} = 20$ m per s and $L = 6000$ km.

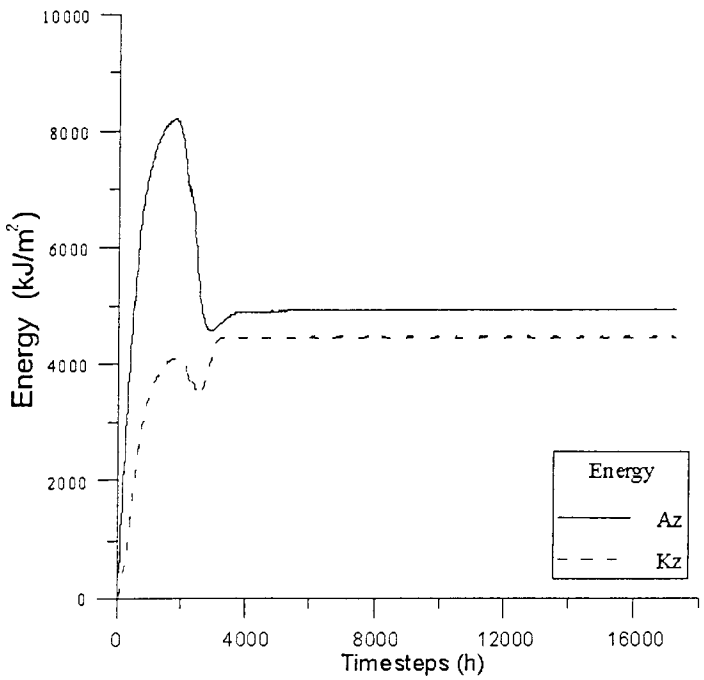

Fig. 3.2. Zonal available and zonal kinetic energies. Parameters as in Fig. 3.1.

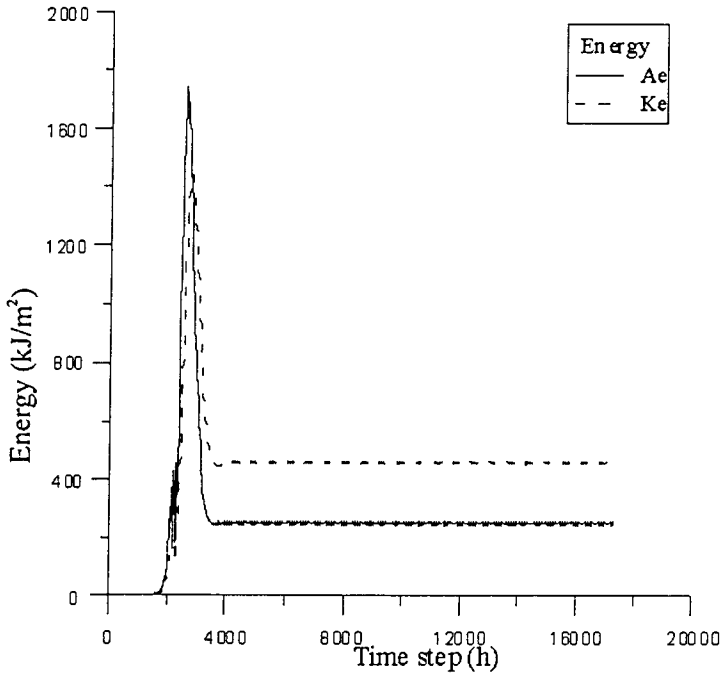

Fig. 3.3. Eddy available and eddy kinetic energies. Parameters as in Fig. 3.1.

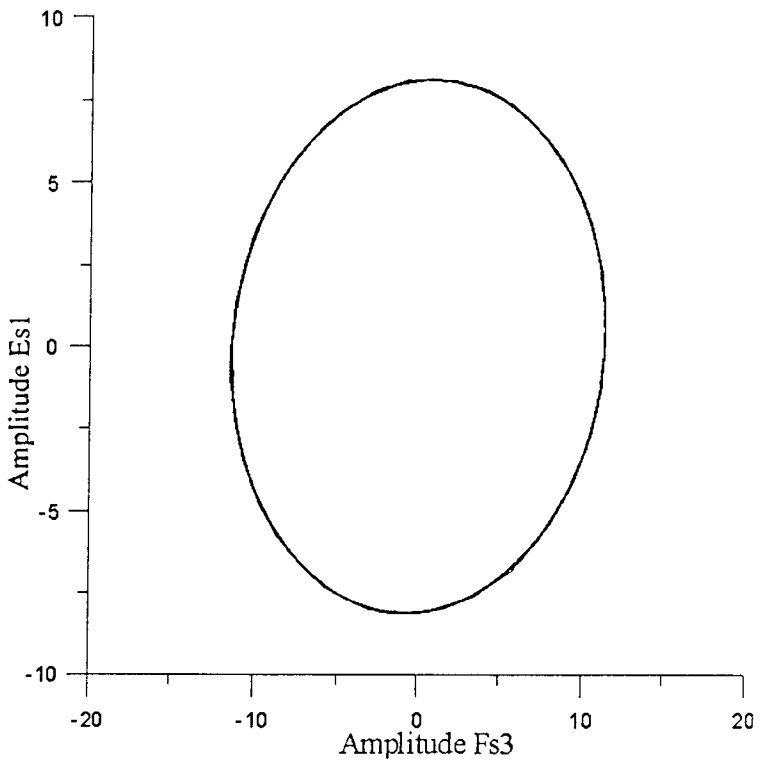

Fig. 3.4. A demonstration of the periodic eddy motion. Parameters as in Fig. 3.1.

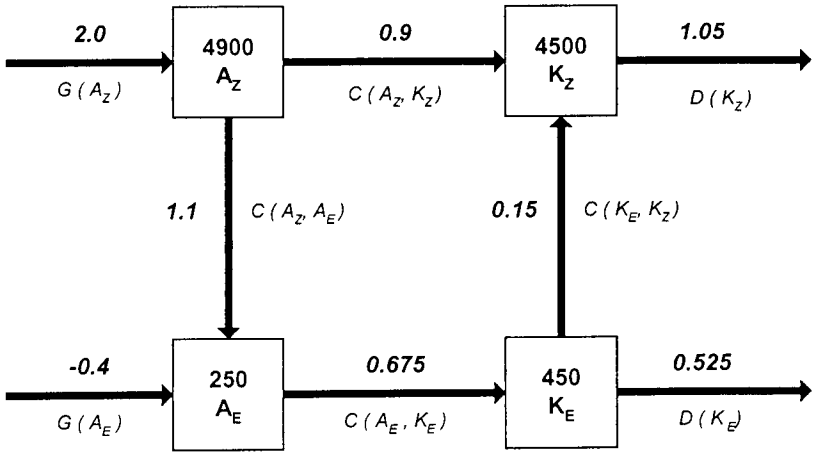

Fig. 3.5. The energy diagram for the experiment described in Fig. 3.1-Fig. 3.4.

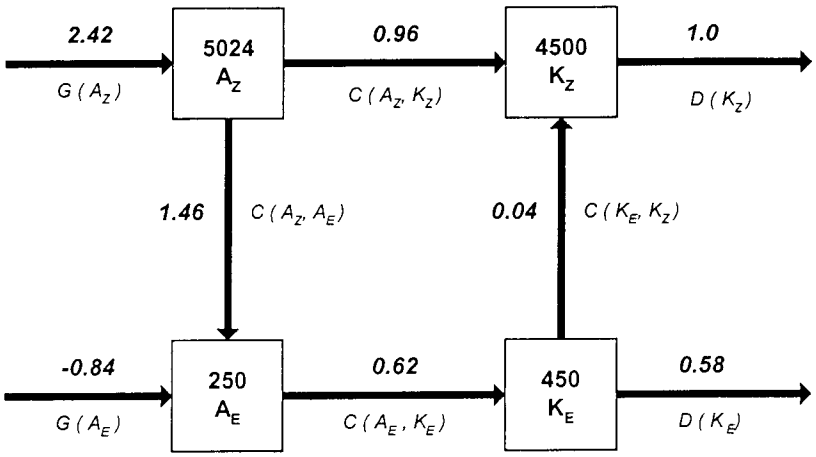

Fig. 3.6. The energy diagram for an experiment with $z_{Tf} = 20$ m per s and $L = 4000$ km.

4. Simulations of blocking situations

It was suggested by Charney and DeVore (1979) using an equivalent barotropic low-order model with Newtonian heating, topographical forcing and dissipations that among the multiple steady states one state was similar to a blocking situation. Their model was formulated on the beta-plane. Independently, Wiin-Nielsen (1979) investigated the multiple steady states of a model forced by heating and including dissipation. He also found that one of the stable steady states could be similar to a blocking situation. This study was formulated on the sphere and therefore used Legendre functions in the formulation of the low-order model. In these studies, dealing only with steady states and their stability, the blocking situation is a result of a nonlinear interaction between the zonal flow and the eddies.

In a later study, inspired to a large degree by the observational investigations of blocking situations by Austin (1980), Christensen (1984) determined that a blocking situation could also be a result of wave-wave interaction among the planetary waves with wave numbers 1, 2 and

3. Christensen and Wiin-Nielsen (1996) used these results to show a better agreement with observations than was found in the case of interactions between the zonal flow and the eddies. These results were obtained by comparing the theoretical eddy kinetic energy amounts with the same quantity obtained by observational studies.

We shall investigate if a blocking pattern may be obtained by integration of the model equations for the 12 component model. If such a schematic simulation can be created, it will be another example of blocking generated by interaction between the zonal flow and the eddies simply because the present model has only one wave number in the west-east direction.

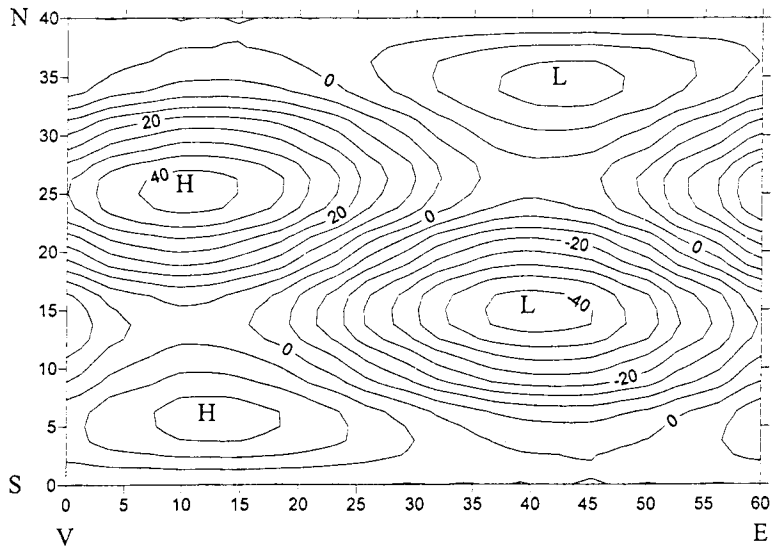

Fig. 4.1. Blocking as an asymptotic steady state with parameters as indicated on the figure.

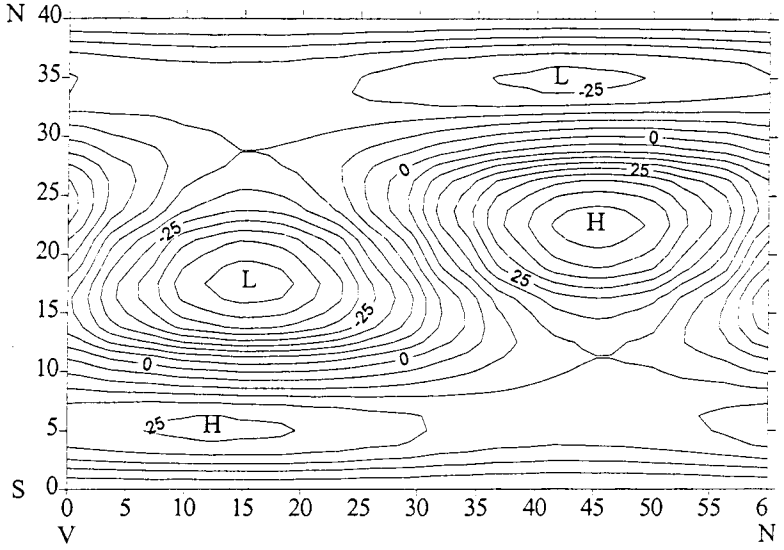

Fig. 4.2. The steady state streamfunction on level 3 for $z_{Tf} = 22$, $w_{Tf} = 15$, $e_{1f} = -15$, $f_{1f} = 15$, $e_{3f} = 20$ and $f_{3f} = -20$, $h_m = 0$.

It turns out that stationary flow pattern similar to blocking may be generated for a large variety of forcing parameters provided that the wavelength is large. We have used 14000 km for the wavelength corresponding to wave number 2 in middle latitudes. Common for the heating functions, resulting in a stationary state similar to blocking is that it has to contain rather large amounts of heating on the eddy components. We show an example where $z_{Tf} = 20$, $w_{Tf} = 10$, $f_{1f} = -20$ and $f_{3f} = 10$, all in m per s, while all the other forcing components are zero. The mountain height was 2000 m, and the south-north length of the channel was 6000 km. It is known from other studies of blocking (Christensen and Wiin-Nielsen, 1996) that the typical length in this direction has to be smaller than the distance from equator to pole. The integration started from an initial state of rest, and the integration was carried out long enough to obtain a steady state. Figure 4.1 shows the result for the streamfunction at level 3, where one recognizes the typical 'omega'-shape characteristic of blocking anticyclones.

In the second example we have used the following values: $z_{Tf} = 22$, $w_{Tf} = 15$, $e_{1f} = -15$, $f_{1f} = 15$, $e_{3f} = 20$ and $f_{3f} = -20$, all in m per s. The topography was excluded in this experiment, i.e. $h_m = 0$. Figure 4.2 displays the steady state streamfunction on level 3, where one once again notices the 'omega'-shape. Figure 4.3 gives the energy conversion $C(K_e, K_z)$ as a function of time for the same case. Based on observational studies the long term mean of this quantity is positive, but for some blocking situations it has been found to be negative, i.e. the conversion is going from K_z to K_e meaning that the zonal kinetic energy must be maintained by the conversion $C\ (A_z,\ K_z)$.

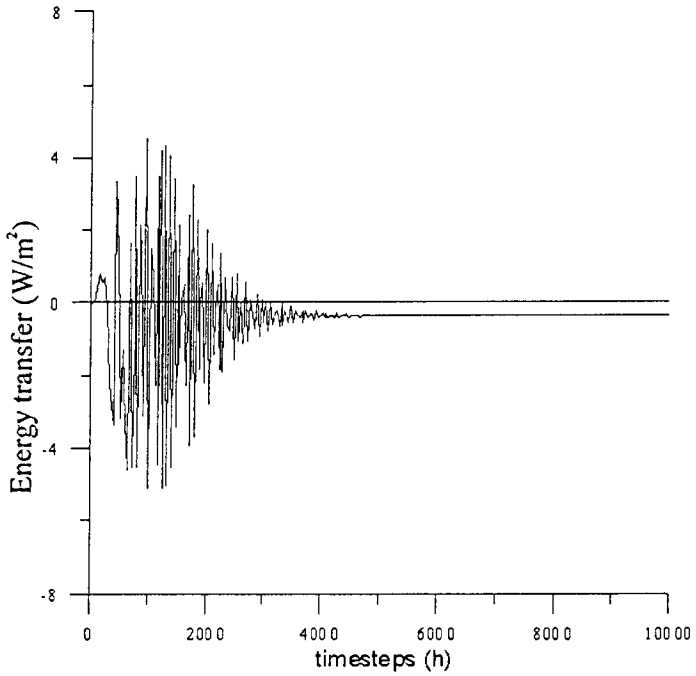

Fig. 4.3. The energy conversion $C(K_e, K_z)$ as a function of time for the case shown in Fig. 4.2.

When the eddy heating values given above are decreased the steady state will eventually disappear. Replacing the steady state one obtains a quasi-periodic oscillation where the energy conversion $C\ (K_e,\ K_z)$ oscillate between small positive and somewhat larger negative values. A possible interpretation of this behavior is that the blocking situations are established from time to time and are maintained for a limited time only after which they break down. Thereafter the

energy conversion from K_e to K_z increases to small positive values, but since the heating that is held constant in time the model atmosphere will again establish a block and so on. Such a development is illustrated in Figure 4.4 showing the energy conversion C $(K_e,\ K_z)$ as a function of time in a case where the heating parameters are: $z_{Tf} = 22$, $w_{Tf} = 15$, $e_{1f} = -7$, $f_{1f} = 7$, $e_{3f} = 12$ and $f_{3f} = -12$.

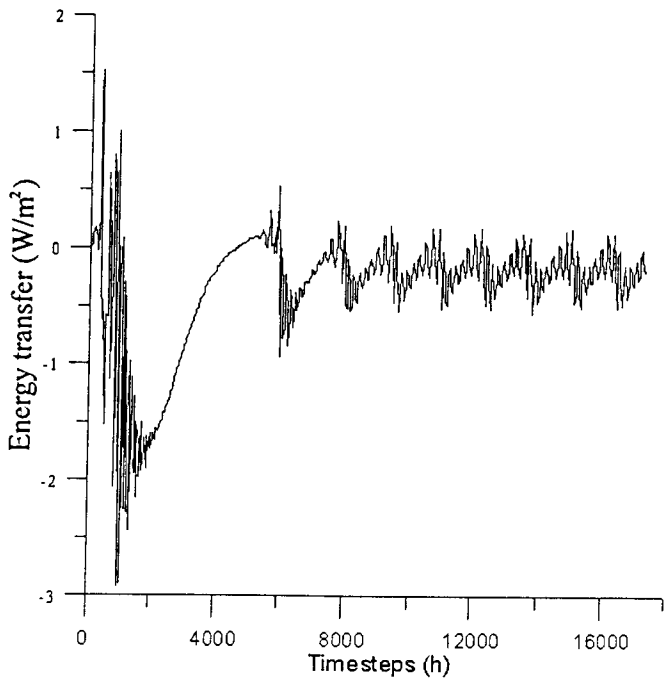

Fig. 4.4. The energy conversion $C(K_e, K_z)$ for a case with $z_{Tf} = 22$, $w_{Tf} = 15$, $e_{1f} = -7$, $f_{1f} = -7$, $e_{3f} = 12$ and $f_{3f} = -12$.

5. Periodic and quasi-periodic nonlinear oscillations

Plaut and Vautard (1994) have made an observational study of occasional low frequency oscillations in the Northern Hemisphere. They find quasi-periods of 30-35 days, 40- 45 days and about 70 days. Such phenomena may be called intermonthly oscillations.

The oscillations with periods of 30-35 days were reproduced by Christensen and Wiin-Nielsen (1996) using a wave-wave interaction, low-order model with six components. A simple model based on a one-dimensional, nonlinear equation of motion with Newtonian forcing was used in a low-order configuration by Wiin-Nielsen (1996) to show that limit cycles with the periods mentioned above could be reproduced by this wave-wave interaction model provided the forcing has the correct order of magnitude. The observed periods may thus be reproduced. On the other hand, different periods appear for other values of the forcing as well, and it remains to be seen why the atmosphere does not contain these periods.

In a second study, Wiin-Nielsen (1997), a nine component model including heating and dissipation, expanded to apply to two-dimensional flow on the beta-plane, was used to investigate the intermonthly oscillations. It was possible to reproduce all the observed periods. In all the models mentioned so far it was assumed that wave-wave interactions take place among waves on the planetary scale, i.e. wave numbers 1, 2 and 3. The time scales found in the theoretical studies mentioned above is thus dictated by the time scales present in cascade processes.

The model treated in the present paper does not contain such interactions, but only interactions between the zonal flow and waves of a given wave number. Any time scales that may be found are therefore related to the conversions of zonal available potential energy to eddy available energy and to the conversion of eddy kinetic to zonal kinetic energy. The first question is therefore if the present model is capable of displaying inter-monthly oscillations.

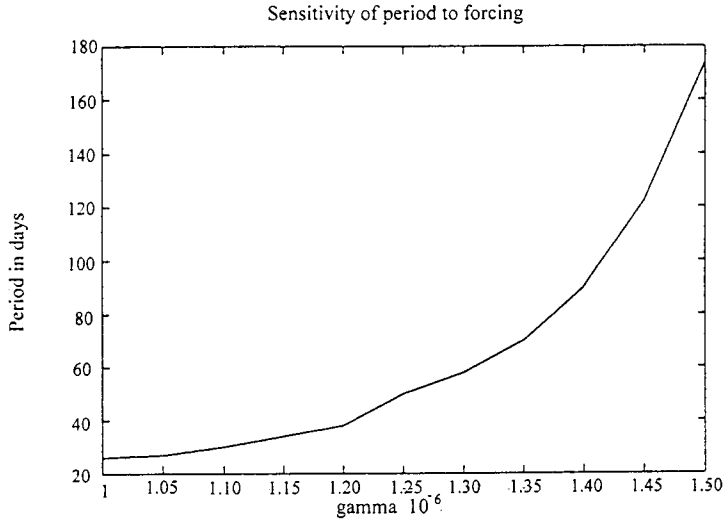

Fig. 5.1. The period, measured in days, as a function of the intensity of the forcing characterized by the parameter $\gamma \times 10^6$.

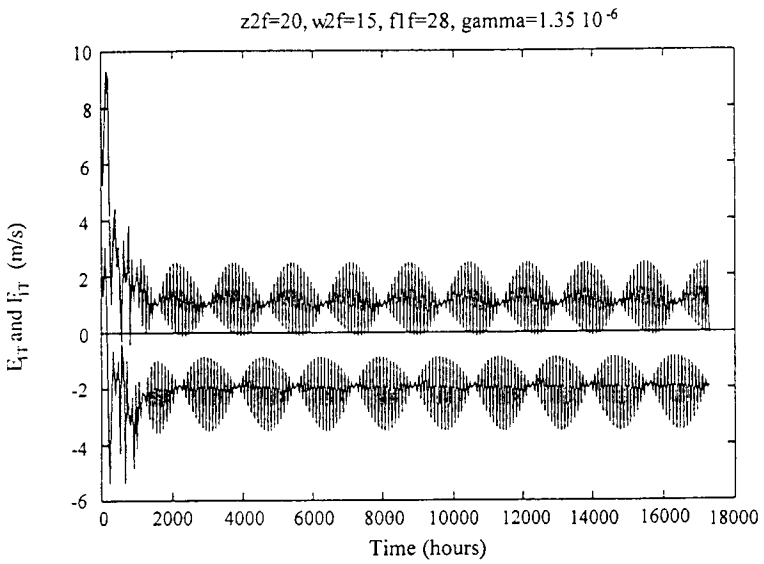

Fig. 5.2. The two components E1T and F1T, measured in m per s, as a function of time. $\gamma = 1.35 \times 10^{-6}$ s^{-1}.

The model was integrated with $z_{Tf} = 20$, $w_{Tf} = 15$ and $f_{1f} = 28$ (all in m per s) while the forcing on the other eddy components was zero. The intensity of the heating may be controlled by changing the coefficient γ in the Newtonian heating. The coefficient was varied from a low value of 1.0×10^{-6} s^{-1} to a high value of 1.5×10^{-6} s^{-1} with changes of 0.05 from one value to the next. For each value of γ periodic variations were found. The period of the oscillations were

found. Figure 5.1 shows the periods as a function of γ. It is seen that the period increases with the intensity of the heating, and that period from 26 to 174 days were determined. Figure (5.2) shows E_{1t} and F_{1t} as a function of time, measured in hours, for a case with $\gamma = 1.35 \times 10^{-6}$ s^{-1}. The period of the oscillation is about 70 days. Figure 5.3 from the same integration shows the energy conversions C $(A_z,\ A_e)$ as a function of time with the same period, while Figure 5.4 displays the energy generations $G(A_z)$ and $G(A_e)$ indicating the same period.

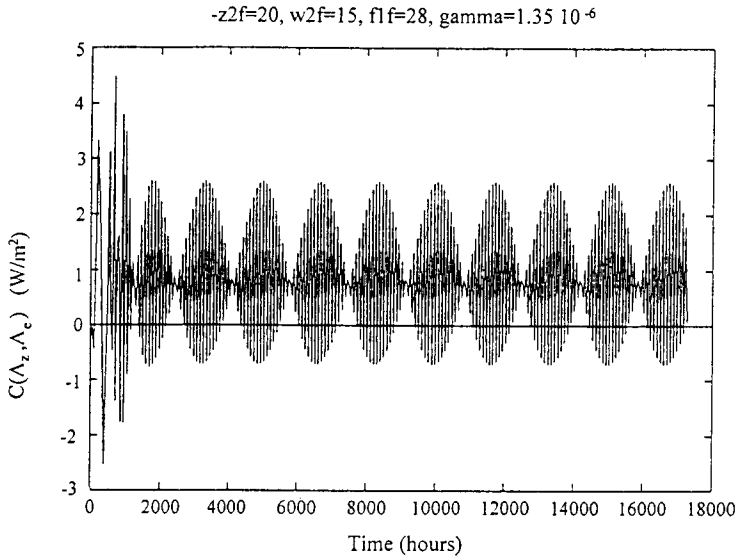

Fig. 5.3. The energy conversion $C(A_z, A_e)$ as a function of time.

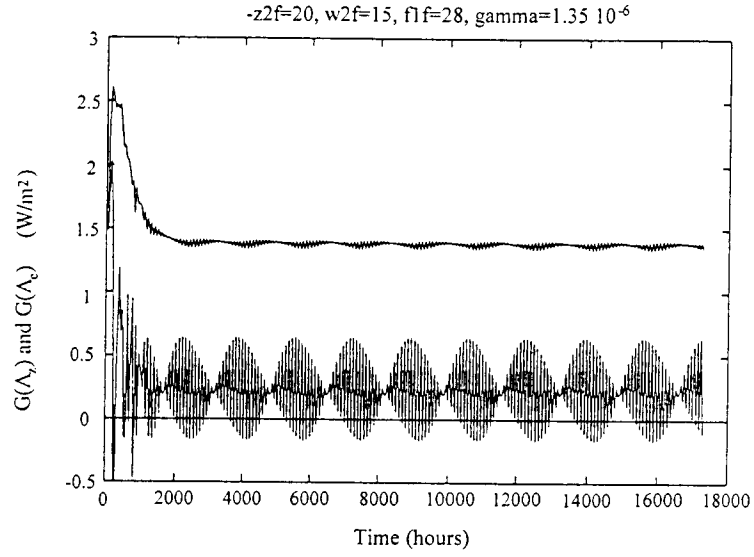

Fig. 5.4. The energy generations $G(A_z)$ and $G(A_e)$ as a function of time.

The length of the channel was equal to 6000 km in the integrations. We are thus in the region of the combined barotropic/baroclinic instability. As indicated by Figure 5.1 the oscillation period is determined by the size of the heating parameter. One should therefore expect that if the forcing on the eddy components are zero we should also find a periodic oscillation in this case. Figure 5.5 is prepared with no heating on any of the wave components and with $\gamma = 1.35 \times 10^{-6}$ s^{-1}. With eddy forcing we found a period of 70 days. Without the eddy forcing the period is reduced to 38 days.

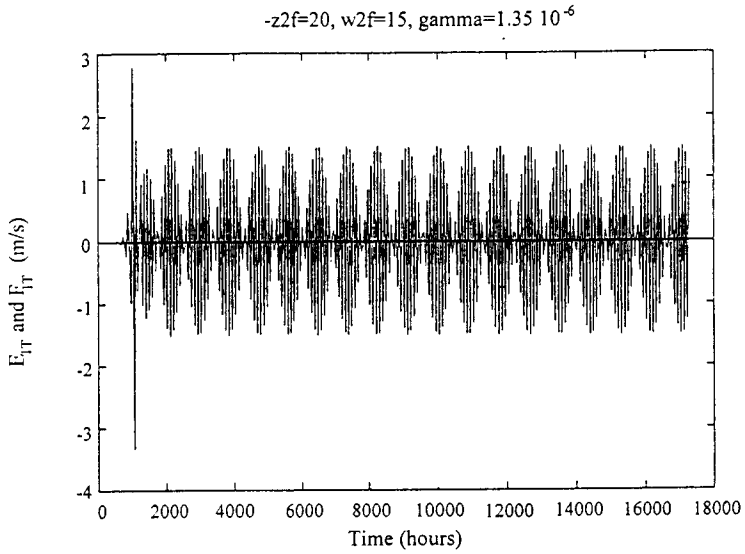

Fig. 5.5. E1T and F1T as functions of time with no eddy forcing.

It therefore appears that the periodic motion found with the present model is of a different kind than the one found using the wave-wave interaction models, simply because the oscillations are found in the region of instability, while the wave-wave interaction models operate on the planetary scale. Thus, it would be desirable to make observational studies to investigate the intermonthly oscillations in wave number space. The other remaining question is to determine why the atmosphere selects the observed periods and not other periods. The answer could probably be obtained by a calculation of the heating fields from observations during the time of the oscillations.

6. Responses to changes in the heating

The atmosphere responds to the changes in the heating fields. The most well known example is the seasonal variations, where we observe a time delay of 1 to 2 months between the astronomical cycle and the seasonal cycle (Wiin-Nielsen, 1970). The present model may be used to investigate some connections between the heating field and the resulting circulation. For these purposes it is more convenient to use the model in the form where the heating parameters are given directly and not in the Newtonian form. In general, the heating field is a function of the two space coordinates x and y. We shall limit ourselves to the case where $h = h(y)$. Within the limits of

the model we express the heating field in the form:

$$h = h_2 \sin(2\lambda y) + h_4 \sin(4\lambda y)$$

$$= h_2(\sin(2\pi\eta) + \epsilon \sin(4\pi\eta))$$

$$\epsilon = \frac{h_4}{h_2};\ \eta = \frac{y}{D} \tag{6.1}$$

By differentiating eq. (6.1) with respect to h we may determine ϵ in such a way that the heating profile has an extreme value at η_e. We find that

$$\epsilon = -\frac{\cos(2\pi\eta_\theta)}{2\cos(4\pi\eta_\theta)} \tag{6.2}$$

Using this value of ϵ we next determine the values of η_e for which the extreme value is a maximum, whereafter we normalize the expression in (6.1) in such a way that the maximum is h_2 which we require to be positive. In addition we decide to use only such heating parameters that the heating is positive in the southern part and negative in the northern part. A small amount of numerical experimentation using (6.1) and (6.2) shows that these requirement are satisfied for $0.16 < \eta_e < 0.34$. The heating profiles for the values 0.17, 0.25 and 0.33 are shown in Figure 6.1. For a channel width of 7000 km the position of the maximum may change by about 1000 km.

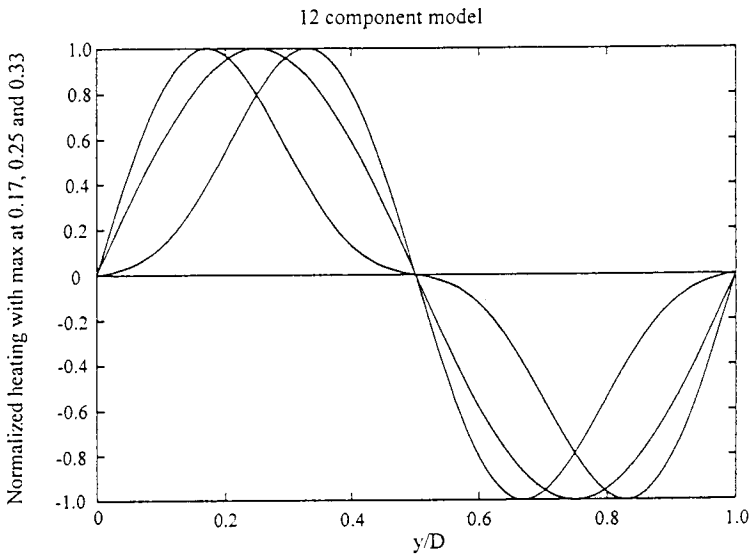

Fig. 6.1. Heating profiles for $\eta_e = 0.17$, 0.25 and 0.33.

For $\eta_e = 0.33$ and $h_2 = 1.5 \times 10^{-3}$ J kg^{-1} s^{-1} we show in Figure 6.2 the streamfunction at level 3 after an integration of 720 days. The state is characterized by a well developed low in the northern half and a high in the southern half. Going to the other extreme, $\eta_e = 0.17$, but with the same value of h_2, we find in Figure 6.3 an entirely different kind of flow pattern showing again the streamfunction at level 3. The waves are now in the middle of the channel and are

less developed. The change between the two kinds of flow pattern seems to appear at $\eta_e = 0.30$ which is the smallest value for which closed isohypses appear in the northern and southern part of the region.

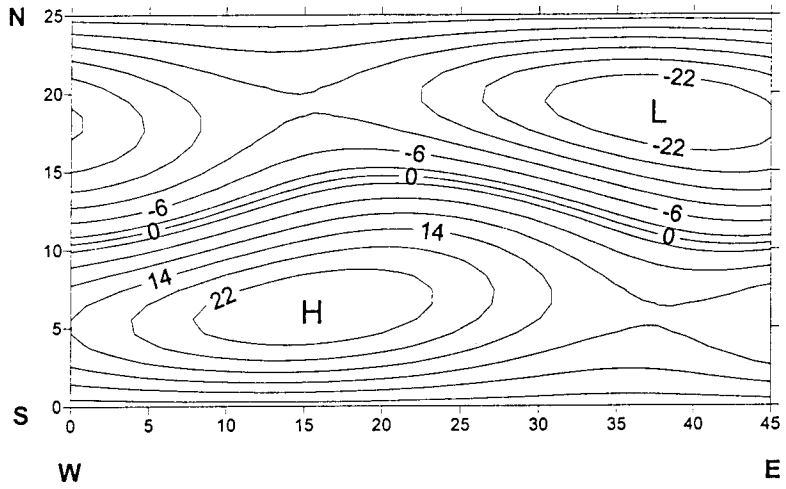

Fig. 6.2. The streamfunction at level 3 for $\eta_e = 0.33$ and $h_2 = 1.5 \times 10^{-3}$ J kg^{-1} s^{-1}

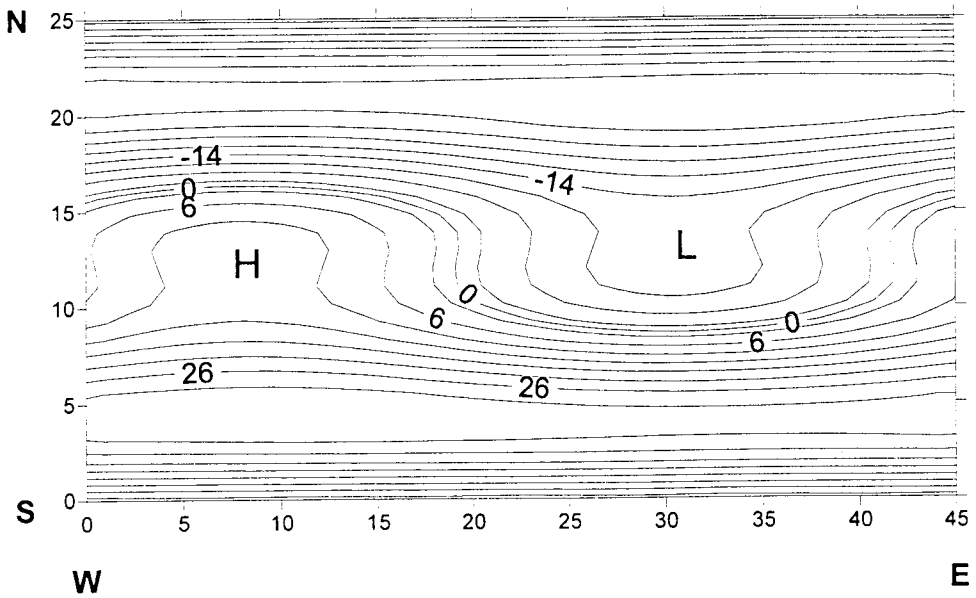

Fig. 6.3. The streamfunction at level 3 for $\eta_e = 0.17$ and the same heating as in Fig. 6.2.

It is also of interest to investigate the importance of the magnitude of h_2 for the final shape of the isohypses. Figure 6.4 shows the streamfunction at level 3 at the same time as the previous figure, but for the value of $h_2 = 1.545 \times 10^{-3}$ J kg^{-1} s^{-1} or 3% larger than the value related to the previous figure and for $\eta_e = 0.33$. We notice the similarity with the map in Figure 6.2, but also the large displacement in the position of the low and the high on the two maps. This experiment shows the large sensitivity to small changes in the initial forcing for the position of the major

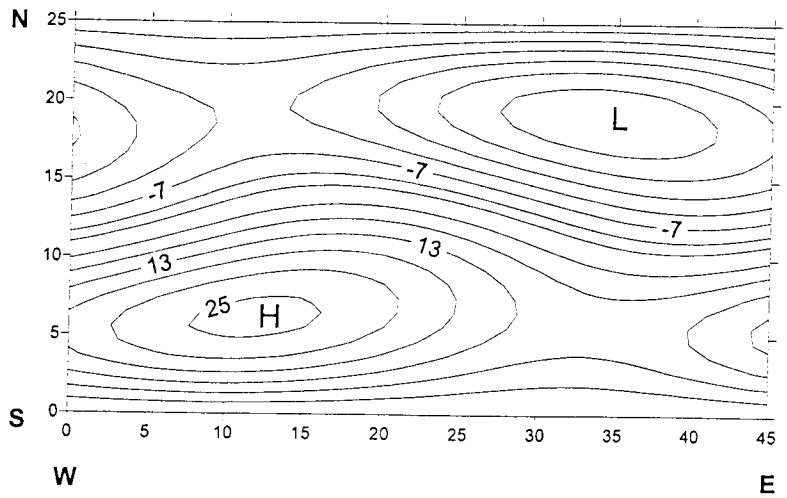

Fig. 6.4. The streamfunction at level 3 for $\eta_e = 0.33$, but $h_2 = 1.545 \times 10^{-3}$ J kg^{-1} s^{-1}.

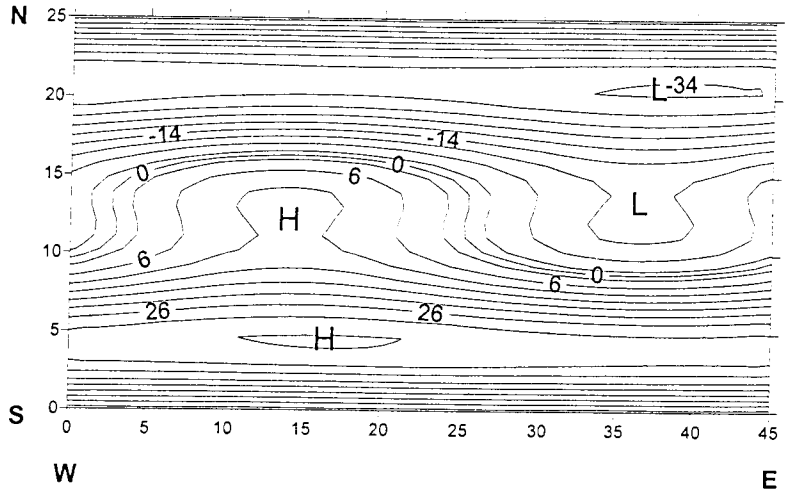

Fig. 6.5. The streamfunction at level 3 for $\eta_e = 0.17$, but $h_2 = 1.545 \times 10^{-3}$ J kg^{-1} s^{-1}.

features in the streamfunction field. A similar difference is found by comparing Figure 6.3 with Figure 6.5. The maximum heating appears in both figures for $\eta_e = 0.17$, but in producing Figure 6.5 the value $h_2 = 1.545 \times 10^{-3}$ J kg^{-1} s^{-1} was used. We have thus demonstrated the sensitivity to the position of the maximum heating and cooling in the south-north direction and the sensitivity to small changes in the forcing in the model.

7. Long waves created by heating and topography

Linear studies by Charney and Eliassen (1949) and Smagorinsky (1953) show that stationary, very long waves are generated by topographical effects and diabatic heating. The topographical forcing, taken in isolation, will generate anticyclonic flow over the mountains and cyclonic flow on the lee side and downstream as measured from the mountain ridge. The diabatic heating

will create cyclonic flow in relation to the maximum heating and anticyclonic flow related to the cooling, but due to the imposed zonal flow in the basic state for the linear perturbation studies the results show also significant phase differences between the heating and cooling and the trough and ridge in the resulting streamfunction.

Several later studies, notably by Döös (1962), have tested the results described above by using different models and by determining the sensitivity of the results to the parameters in the model. It has for example been shown by Derome (1968) that the amplitude of the stationary flow is sensitive to the width of the channel when the investigation uses a beta-plane.

In this section we shall use the low-order model to generalize the linear studies. To simulate the two effects in the low-order nonlinear model it is impossible to separate them completely because the topographical effect requires a flow over the mountains, and this flow is generated in the model by the differential heating in the meridional direction. On the other hand, these integrations of the model equations use a large length of the channel, say 14000 km. On this scale the model will not generate transient waves by barotropic/baroclinic instability, and the generated waves are then due to the topography. It may be useful to imagine that the rectangular region is divided in a western continental region and an eastern oceanic region, but with only one longitudinal wave number the topography will stretch over the whole domain.

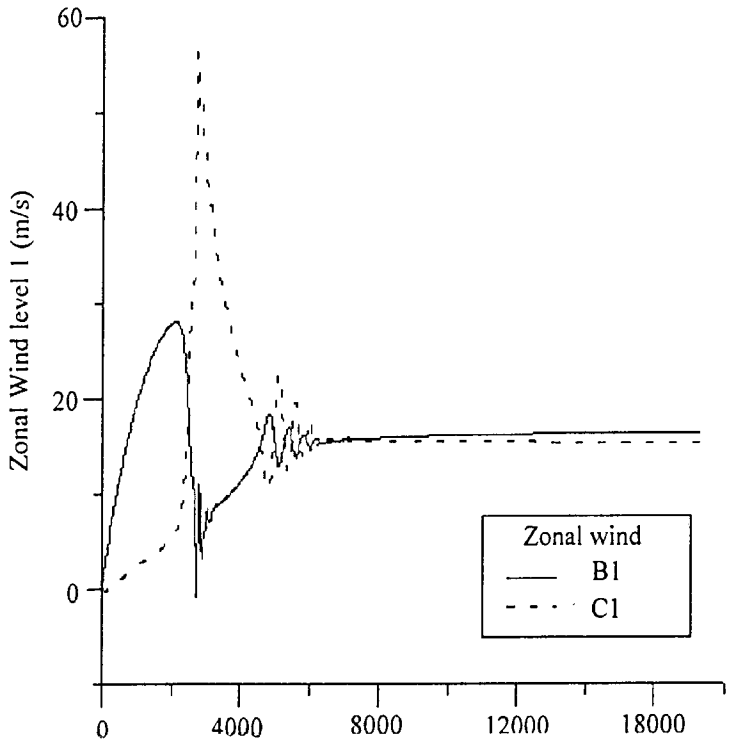

Fig. 7.1. Zonal wind components B_1 and C_1 as a function of time for $h_2 = 2 \times 10^{-3}$ J kg^{-1} s^{-1} and $h_m = 5000$ m.

In the experiments we use a heating specified by $h_2 = 2 \times 10^{-3}$ J kg^{-1} s^{-1} and a mountain height of $h_m = 5000$ m. Figure 7.1 indicates that an asymptotic steady state is reached after about 250 days. As shown by Figure 7.2 the result is a cyclonic circulation over the western part and an anticyclonic circulation over the eastern part.

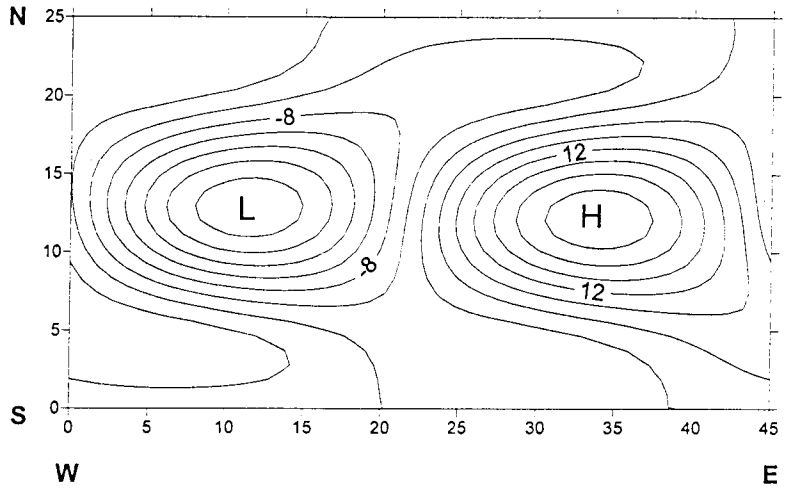

Fig. 7.2. Streamfunction at level 3 for the parameters given in Fig. 7.1.

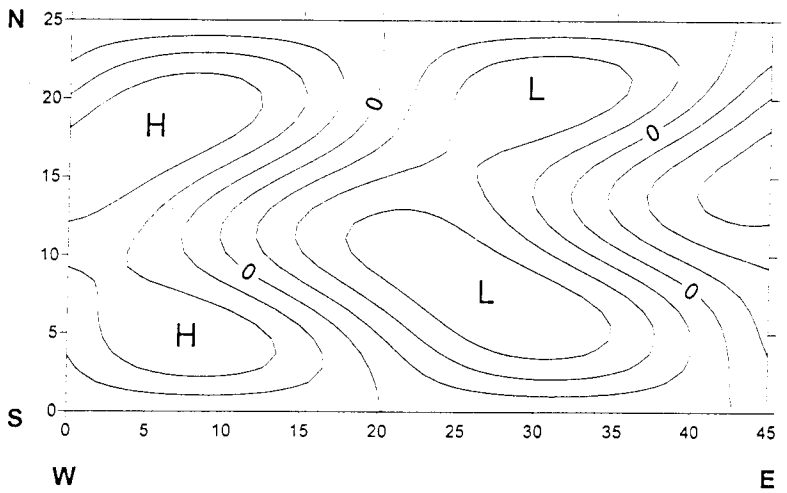

Fig. 7.3. Streamfunction at level 3 for $hf_1 = hf_3 = -9.0 \times 10^{-4}$ J kg^{-1} s^{-1}, $h_m = 0$, and no heating from other components.

To simulate the heating effect we set the heating parameters to $h_{1f} = h_{3f} = -9.0 \times 10^{-4}$ J kg^{-1} s^{-1} , while the mountain parameter and all other eddy components of the heating field are set to zero. With these specifications there will be cooling over the western and heating over the eastern part of the region. The integration to a steady state is shown in Figure 7.3. The essential part of the flow is an anticyclonic circulation to the west and a cyclonic circulation to the east. Figure 7.4 shows what happens when we change the sign on the two heating components. The cyclonic circulation is to the west and the anticylonic to the east.

In the following integrations we shall include topographical and heating effects in the model. Many combinations are possible. We shall restrict ourselves to a few cases with $h_m = 5$ km. The first case has cooling over the western side and heating over the eastern side with the values $h_{1f} = h_{3f} = -9.0 \times 10^{-4}$ J kg^{-1} s^{-1}. The integration leads to a steady state, shown in Figure 7.5. In this case we expect that the heating effect and the topographical effect will

reinforce each other, since both of them will tend to create anticyclonic flow in the western and cyclonic flow in the eastern part. This expectation is verified by Figure 7.5. In the next case we change the sign on the two heating component given above. In this case the two effects will counteract each other, and the final result will depend on their relative strengths. Figure 7.6 shows a cyclonic circulation near the middle of the channel and somewhat to the east of the coastline located at $x = 24$. Over the western half we find anticyclonic flow in the middle of the channel, but the cyclonic circulation stretches into the north-westerly region. Therefore, we conclude that the topographical effect dominates over the heating effect.

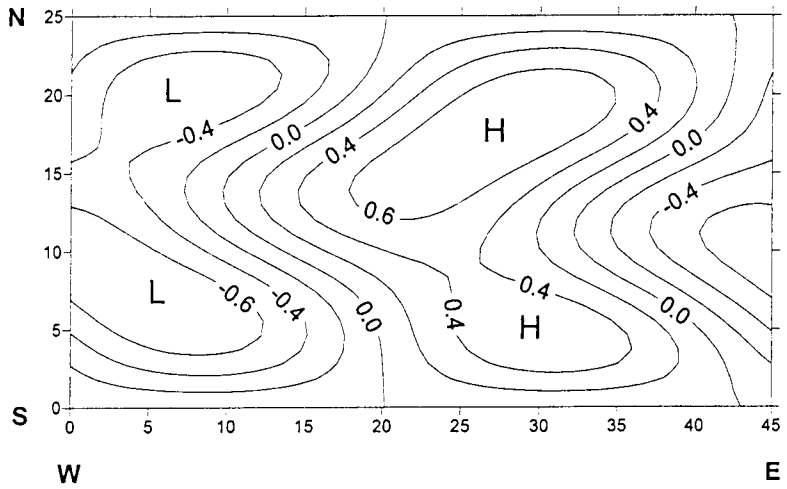

Fig. 7.4. As Fig. 7.3, but the sign has been changed on the two heating components.

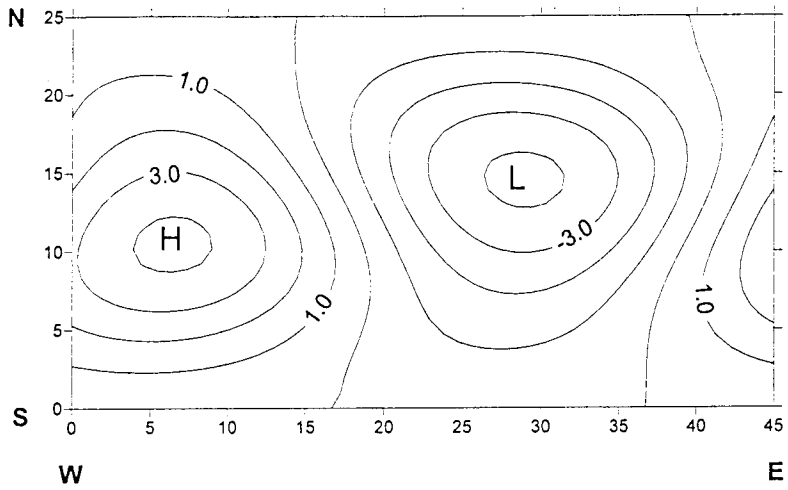

Fig. 7.5. The streamfunction at level 3 for $hf_1 = hf_3 = -9.0 \times 10^{-4}$ and $h_m = 5000$ m.

In the final experiment in this section we increase the forcing to the values $h_{1f} = h_{3f} = 4.8 \times 10^{-3}$ J kg^{-1} s^{-1}. The steady state is given in Figure 7.7. In this case the mountaing effect still dominates since the western part has anticyclonic flow, while the eastern part has cyclonic flow.

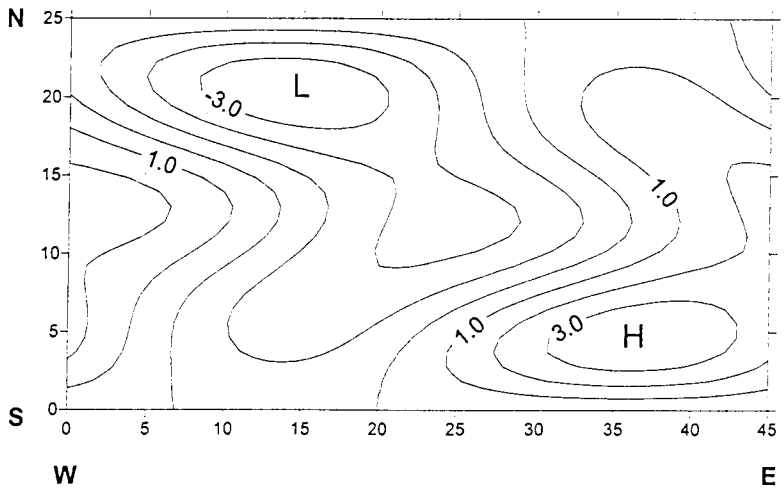

Fig. 7.6. As Fig. 7.5, but the sign has been changed on the two heating components.

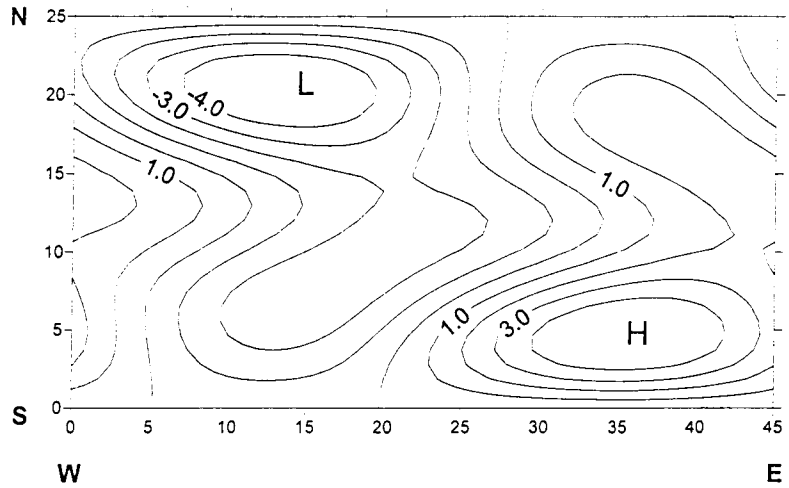

Fig. 7.7. Streamfunction at level 3 for $hf_1 = hf_3 = 4.8 \times 10^{-3}$ J kg^{-1} s^{-1} and $h_m = 5000$ m.

The cases in this section may be considered as an expansion of the linear theory into the nonlinear domain, where as usual one has to rely on steady states obtained as asymptotic states after a numerical integration of sufficient length.

8. Summary and concluding remarks

The purpose of the paper has been to use a 12 component, low-order, quasi-nondivergent, two level model to simulate a number of nonlinear atmospheric processes. The model is a minimal model in the sense that models with fewer components will not be able to include both the meridional transports of sensible heat and of momentum. At the same time, the model permits a calculation of all energy generations, conversions and dissipations cycle as given by the atmospheric four box energy diagram. The model may have heating on all components expressed

either directly or through a Newtonian heating. Topographical forcing is also included in the model, but the topography is represented by a single trigonometric term.

All investigations have been done by numerical experiments, and no analytical work has been included. The long integrations have been carried out using the Heun scheme for the time integrations, normally with a time step of 1 hour. For each integration it is possible to calculate the energetics of the model and to obtain all quantities as functions of time. The program also permits the production of maps of the various field distributions.

The model with its few components as compared to any large-scale, global model of the general circulation of the atmosphere is still capable of illustrating a number of important atmospheric processes, e.g. the creation of atmospheric waves by barotropic/baroclinic instabilities, the development of these waves in the nonlinear domain, a study of the creation of blocking structures through nonlinear interactions between the zonal flow and the eddies, the atmospheric response to changes in the heating, both with respect to the intensity of the forcing and to changes in the position of the maximum heating in the south-north direction, with the result that a maximum heating located well to the south will result in an entirely different flow configuration compared with a more northerly position of the maximum heating, and, finally, a study of the creation of long stationary waves as influenced by both diabatic heating and topography.

Some important processes are naturally excluded from the model. With only one wave number in the zonal direction and a few components to describe the meridional behavior the model cannot represent any cascade processes of any kind. Thus, the produced maps are of a schematic character.

It has not been attempted to ascribe the heating to specific physical processes. The reason is that any attempt in this direction will lead to additional time-dependent variables such as a description of moisture, clouds, sea-surface temperatures, etc. A move in this direction seems to be counterproductive to the main idea embedded in the model.

APPENDIX 1

In this appendix we discuss the 12 component model and give the equations and constants entering the equations. The model is a two level, quasi-nondivergent model based on a vorticity equation for the vertical mean flow which may be identified with the 500 hPa level and a thermal vorticity equation that describes the development in a layer with a pressure difference of 250 hPa. The region is rectangular with the length L in the west-east direction and the width D in the south-north direction. We use the notation $k = 2\pi/L, \lambda = \pi/D$ and $q^2 = (2f_o^2)/(\sigma P^2)$, where the last quantity is the stability parameter. In all calculations we have used $q^2 = 4 \times 10^{-12}$ m^{-2} and a value of $\beta = 1.6 \times 10^{-11}$ m^{-1} s^{-1}, where β is the variation of the Coriolis parameter with latitude. We recall that Ψ_* and Ψ_T are half the sum and half the difference between the streamfunctions at 250 hPa and 750 hPa.

The zonal parts of the streamfunctions are given by:

$$(\Psi_*)_z = \frac{z_*}{2\lambda}\sin(2\lambda y) + \frac{w_*}{4\lambda}\sin(4\lambda y) \tag{1}$$

$$(\Psi_T)_z = \frac{z_T}{2\lambda}\sin(2\lambda y) + \frac{w_T}{4\lambda}\sin(4\lambda y) \tag{2}$$

The eddy parts of the streamfunction are given by

$$(\Psi_*)_E = \frac{1}{k}\sin(\lambda y)(x_{*1}\cos(kx) + y_{*1}\sin(kx))$$

$$+\frac{1}{k}\sin(3\lambda y)(x_{*3}\cos(kx) + y_{*3}\sin(kx)) \tag{3}$$

$$(\Psi_T)_E = \frac{1}{k}\sin(\lambda y)(x_{T1}\cos(kx) + y_{T1}\sin(kx))$$

$$+\frac{1}{k}\sin(3\lambda y)(x_{T3}\cos(kx) + y_{T3}\sin(kx)) \tag{4}$$

The following notations for the transport quantities, appearing in the final equations, are introduced:

$$T_h = x_{T1}y_{*1} - x_{*1}y_{T1}$$

$$M_* = x_{*1}y_{*3} - x_{*3}y_{*1}$$

$$M_T = x_{T1}y_{T3} - x_{T3}y_{T1}$$

$$M_T^* = x_{T3}y_{*1} - x_{*1}y_{T3}$$

$$M_*^T = x_{*3}y_{T1} - x_{T1}y_{*3} \tag{5}$$

$$Q = \frac{\lambda^2}{k^2}$$

$$R = \frac{\beta}{k^2}$$

$$S_1 = \frac{q^2}{\lambda^2}$$

$$S_2 = \frac{q^2}{k^2} \tag{6}$$

The twelve equations are:

$$\frac{dz_*}{dt} = -a_1(M_* + M_T) \tag{7}$$

$$\frac{dw_*}{dt} = a_1(M_* + M_T) \tag{8}$$

$$\frac{dx_{*1}}{dt} = a_2(z_* y_{*1} + z_T y_{T1}) + a_3(z_* y_{*3} + z_T y_{T3})$$

$$+a_4(w_* y_{*3} + w_T y_{T3}) + b_1 y_{*1} \tag{9}$$

$$\frac{dy_{*1}}{dt} = -a_2(z_* x_{*1} + z_* x_{T1}) - a_3(z_* x_{*3} + z_T x_{T3})$$

$$-a_4(w_* x_{*3} + w_T x_{T3}) - b_1 x_{*1} \tag{10}$$

$$\frac{dx_{*3}}{dt} = a_5(w_* y_{*1} + w_T y_{T1}) - a_6(z_* y_{*1} + z_T y_{T1}) + b_2 y_{*3} \tag{11}$$

$$\frac{dy_{*3}}{dt} = -a_5(w_* x_{*1} + w_T x_{T1}) + a_6(z_* x_{*1} + z_T x_{T1}) - b_2 x_{*3} \tag{12}$$

$$\frac{dz_T}{dt} = a_7 M_T^* + a_8 M_*^T - a_4 T_h \tag{13}$$

$$\frac{dw_T}{dt} = -a_7 M_T^* + a_8 M_*^T \tag{14}$$

$$\frac{dx_{T1}}{dt} = a_{11}z_*y_{T1} + a_{12}z_*y_{T3}a_{13}w_*y_{T3}$$

$$+a_{14}z_Ty_{*1} + a_{15}z_Ty_{*3} + a_{16}w_Ty_{*3} + b_3y_{T1} \tag{15}$$

$$\frac{dy_{T1}}{dt} = -a_{11}z_*x_{T1} - a_{12}z_*x_{T3} - a_{13}w_*x_{T3}$$

$$-a_{14}z_Tx_{*1} - a_{15}z_Tx_{*3} - a_{16}w_Tx_{*3} - b_3x_{T1} \tag{16}$$

$$\frac{dx_{T3}}{dt} = a_{17}w_*y_{T1} - a_{18}z_*y_{T1}$$

$$+a_{19}w_Ty_{*1} - a_{20}z_Ty_{*1} + b_4y_{T3} \tag{17}$$

$$\frac{dy_{T3}}{dt} = a_{17}w_*x_{T1} + a_{18}z_*x_{T1}$$

$$-a_{19}w_Tx_{*1} + a_{20}z_Tx_{*1} - b_4x_{T3} \tag{18}$$

The list of constants for each integration is:

$$a_1 = 2kQ \tag{19}$$

$$a_2 = k\frac{3Q-1}{2(1+Q)} \tag{20}$$

$$a_3 = k\frac{5Q+1}{2(1+Q)} \tag{21}$$

$$a_4 = k\frac{7Q-1}{2(1+Q)} \tag{22}$$

$$a_5 = k\frac{15Q - 1}{2(1 + 9Q)} \tag{23}$$

$$a_6 = k\frac{3Q - 1}{2(1 + 9Q)} \tag{24}$$

$$a_7 = k\frac{2Q + S_1/4}{1 + S_2/4} \tag{25}$$

$$a_8 = k\frac{2Q - S_1/4}{1 + S_2/4} \tag{26}$$

$$a_9 = k\frac{S_1/4}{1 + S_2/4} \tag{27}$$

$$a_{10} = k\frac{2Q + S_1/4}{1 + S_2/16} \tag{28}$$

$$a_{11} = k\frac{3Q - S_1 - 1}{2(1 + Q + S_1)} \tag{29}$$

$$a_{12} = k\frac{5Q + S_1 + 1}{2(1 + Q + S_1)} \tag{30}$$

$$a_{13} = k\frac{7Q - S_1 - 1}{2(1 + Q + S_1)} \tag{31}$$

$$a_{14} = k\frac{3Q + S_1 - 1}{2(1 + Q + S_1)} \tag{32}$$

$$a_{15} = k\frac{5Q + S_1 + 1}{2(1 + Q + S_1)} \tag{33}$$

$$a_{16} = k\frac{7Q + S_1 - 1}{2(1 + Q + S_1)} \tag{34}$$

$$a_{17} = k\frac{15Q + S_1 - 1}{2(1 + 9Q + S_1)} \tag{35}$$

$$a_{18} = k\frac{3Q - S_1 - 1}{2(1 + 9Q + S_1)} \tag{36}$$

$$a_{19} = k\frac{15Q + S_1 - 1}{2(1 + 9Q + S_1)} \tag{37}$$

$$a_{20} = k\frac{3Q + S_1 - 1}{2(1 + 9Q + S_1)} \tag{38}$$

$$b_1 = \frac{R}{1 + Q} \tag{39}$$

$$b_2 = \frac{R}{1 + 9Q} \tag{40}$$

$$b_3 = \frac{R}{1 + Q + S_1} \tag{41}$$

$$b_4 = \frac{R}{1 + 9Q + S_1} \tag{42}$$

The twelve equations for the model as given above apply to the case of no forcing, no dissipation and no mountains. In general these effects should of course be present, but for convenience we give below separately the expressions that have to be added to the right hand side of each equation.

I Heating terms

The heating in the model is of a Newtonian type. Denoting an arbitrary dependent variables by v and the forcing on this component by v_f one has to add to equations (13) to (18) incl. a term of the form:

$$\gamma(v_f - v)$$

Example: For the variable z_T one adds the term:

$$\gamma(z_{Tf} - z_T)$$

The standard value of $\gamma = 1.0 \times 10^{-6}$ s^{-1}.

II Dissipation terms

For the first six equations one has to add the terms:

1: $-\varepsilon(z_* - 2z_T)$
2: $-\varepsilon(w_* - 2w_T)$
3: $-\varepsilon(x_{1*} - 2x_{1T})$
4: $-\varepsilon(y_{1*} - 2y_{1T})$
5: $-\varepsilon(x_{3*} - 2x_{3T})$
6: $-\varepsilon(y_{3*} - 2y_{3T})$

The standard value of $\varepsilon = 2.0 \times 10^{-6}$ s^{-1}.

For the last six equations one has to add the terms:

7: $[\varepsilon(z_* - 2z_T) - \varepsilon_T z_T]/(1 + S_2/4)$
8: $[\varepsilon(w_* - 2w_T) - \varepsilon_T w_T]/(1 + S_2/16)$
9: $[\varepsilon(x_{1*} - 2x_{1T}) - \varepsilon_T x_{1T}](1 + Q)/(1 + Q + S_1)$
10: $[\varepsilon(y_{1*} - 2y_{1T}) - \varepsilon_T y_{1T}](1 + Q)/(1 + Q + S_1)$
11: $[\varepsilon(x_{3*} - 2x_{3T}) - \varepsilon_T x_{3T}](1 + 9Q)/(1 + 9Q + S_1)$
12: $[\varepsilon(y_{3*} - 2y_{3T}) - \varepsilon_T y_{3T}](1 + 9Q)/(1 + 9Q + S_1)$

The standard value of $\varepsilon_T = 6.0 \times 10^{-1}$ s^{-1}.

III Mountain terms

To keep the model as simple as possible we shall not treat the general problem, but shall

restrict the mountains to have the form:

$$h = h_m \sin(\lambda y) \sin(kx) \tag{43}$$

This means that we consider a case where the continent with the mountain is in the western part of the region. As in the previous case we make a list of the terms that should be added to the right hand side of the 12 equations, i.e. (7) to (18):

1: $-c_m h_m (x_{1*} - x_{3*} - x_{1T} + x_{3T})/4$
2: $-c_m h_m (x_{3*} - x_{3T})/4$
3: $c_m h_m (z_* - z_T)/(2(1+Q))$
4: 0
5: $-c_m h_m (z_* - w_* - z_T + w_T)/(2(1+9Q))$
6: 0
7: $c_m h_m (x_{1*} - x_{3*} - x_{1T} + x_{3T})/(2(4+S_2))$
8: $c_m h_m (x_{3*} - x_{3T})/(16+S_2))$
9: $-c_m h_m (z_* - z_T)/(2(1+Q+S_1))$
10: 0
11: $c_m h_m (z_* - w_* - z_T + w_T)/(2(1+9Q+S_1))$
12: 0

The constant $c_m = g f_o/(RT_o) = 1.1856 \times 10^{-8}$ m^{-1} s^{-1}.

IV Typical values of other constants

D $= 7.0 \times 10^6$ m (the width of the region)

$\beta = 1.6 \times 10^{-11}$ m^{-1} s^{-1} ($\beta = 2\Omega \cos(\text{lat})/a$ with $\Omega = 7.29 \times 10^{-5}$ s^{-1}, $a = 6371$ km, lat $= 45$ degrees.

R $= 287.0$ m^2 s^{-2} K^{-1}

g $= 9.8$ m s^{-2}

q$^2 = 4.0 \times 10^{-12}$ m^{-2}

Appendix 2

Sect.	$Lx10^3$ km	z_{Tf}	w_{Tf}	e_{1f}	f_{1f}	e_{3f}	f_{3f}	h_m
3	6	20	0	0	0	0	0	0
3	4	20	0	0	0	0	0	0
3	14	20	0	0	0	0	0	0
3	1	20	0	0	0	0	0	0
3	2	20	0	0	0	0	0	0
4	14	20	10	0	-20	0	10	2000
4	14	22	15	-15	15	20	-20	0
4	14	22	15	-7	7	12	-12	0
5	6	20	15	0	28	0	0	0
5	6	20	15	0	0	0	0	0
7	14	13.3	0	0	0	0	0	5000
7	14	13.3	0	-6	0	-6	0	0
7	14	13.3	0	-6	0	-6	0	5000
7	14	13.3	0	6	0	6	0	5000
7	14	13.3	0	32.1	0	32.1	0	5000

Note: The last five experiments were done specifying the heating. The values in the table has been found by using the conversion:

$$u_f = \frac{q^2\kappa}{2\lambda f_o \gamma} h$$

with D = 6000 km, $\gamma = 1.5 \times 10^{-6}$ s^{-1} and standard values for the other parameters.

REFERENCES

Austin, J. F., 1980. The blocking of middle latitude westerly winds by planetary waves, *Quart. Jour. of the Roy. Met. Soc.*, **106**, 327-350.

Charney, J. G., 1959. On the general circulation of the atmosphere, The Atmosphere and Sea in Motion, The Rockefeller Institute Press, 178-193.

Charney, J. G. and A. Eliassen, 1949. A numerical method for predicting the perturbations of the middle latitude westerlies, *Tellus*, **1**, 38-54.

Charney, J. G. and J. G. DeVore, 1979. Multiple flow equilibria in the atmosphere and blocking, *J. Atmos. Sci.*, **36**, 1205-1216.

Christensen, C. Wiin, 1984. Blocking, M. Sc. diss, Dept. of Geophys., Univ. of Copenhagen, 106 pp.

Christensen, C. Wiin and A. Wiin-Nielsen, 1996. Blocking as a wave-wave interaction, *Tellus*, **48A**, 254-271.

Derome, J. F., 1968. The maintenance of the time-averaged state of the atmosphere, Ph.D. thesis, Univ. of Michigan, 129 pp.

Döös, B. R., 1962. The influence of exchange of sensible heat with the Earth's surface on the planetary flow, *Tellus*, **14**, 133-147.

Lorenz, E. N., 1955. Available potential energy and the maintenance of the general circulation, *Tellus*, **7**, 157-167.

Lorenz, E. N., 1960. Maximum simplification of the dynamic equations, *Tellus*, **12**, 243-254.

Lorenz, E. N., 1962. Simplified dynamic equations applied to rotating basin experiments, *J. Atmos. Sci.*, **19**, 39-51.

Lorenz, E. N., 1963. Deterministic non-periodic flow, J. Atmos. Sci., **20**, 130-141.

Lorenz, E. N., 1963. The mechanics of vacillation, *J. Atmos. Sci.*, **20**, 448-464.

Marsh, N., I. A. Mogensen and A. Wiin-Nielsen, 1995. On the stability of single and double jets, *Geophysica*, **31(2)**, 47-57.

Phillips, N. A., 1956. The general circulation of the atmosphere: A numerical experiment, *Quart. Jour. of the Roy. Met. Soc.*, **82**, 123-164.

Plaut, G. and R. Vautard, 1994. Spells of low-frequency oscillations and weather regimes in the Northern Hemisphere, *J. Atmos. Sci.*, **51**, 210-236.

Platzman, G. W., 1960. The spectral form of the vorticity equation, *Jour. Meteor.*, **17**, 635-644.

Smagorinsky, J., 1953. The dynamical influence of large-scale heat sources and sinks on the quasi-stationary mean motions in the atmosphere, *Quart. Jour. of the Roy. Met. Soc.*, **97**, 342-386.

Stuart, J. T., 1960. On the nonlinear mechanics of wave disturbances in stable and unstable parallel flow, Part 1, The basic behavior in plane Poisuille flow, *J. of Fluid Mech.*, **9**, 353-370.

Watson, J., 1960. On the nonlinear mechanics of wave disturbances in stable and unstable parallel flow, Part 2, The development of a solution for plane Poiseuille flow and plane Couette flow, *J. of Fluid Mech.*, **9**. 371-380.

Wiin-Nielsen, A., 1961. On short- and long-term variations in quasi-barotropic flow, *Mo. Wea. Rev.*, **89**, 461-476.

Wiin-Nielsen, A., 1970. A theoretical study of the annual variation of atmospheric energy, *Tellus*, **22**, 1-16.

Wiin-Nielsen, A., 1975. Predictability and climate variation illustrated by a low-order system, ECMWF Seminar on Scientific Foundation of Medium-Range Forecasts, 258-306.

Wiin-Nielsen, A., 1979. Steady states and stability properties of a low-order, barotropic system with forcing and dissipation, Tellus, **31**, 375-386.

Wiin-Nielsen, A., 1990. A study of large-scale atmospheric waves and the response to external forcing, *Geophysica*, **26**, 1-28.

Wiin-Nielsen, A., 1991a. Comparisons of low-order atmospheric dynamic systems, *Atmósfera*, **5**, 135-155.

Wiin-Nielsen, A., 1991b. Low-order baroclinic models forced by meridional and zonal heating, *Geophysica*, **27**, 13-40.

Wiin-Nielsen, A., 1994a. On equilibrium between orography and atmosphere, *Atmósfera*, **7**, 3-20.

Wiin-Nielsen, A., 1994b. Nonlinear studies of quasi-geostrophic systems, *Physica D*, **77**, 33-59.

Wiin-Nielsen A., 1996. A note on longer term oscillations in the atmosphere, *Atmósfera*, **9**, 222-240.

Wiin-Nielsen, A., 1997. On intermonthly oscillations in the atmosphere, Part II, *Atmósfera*, **10**, 23-42.

Yang, C.-H., 1967. Nonlinear aspects of large-scale motion in the atmosphere, Ph. D. Thesis, University of Michigan, 173 pp.